

Lawrence Berkeley National Laboratory

Lawrence Berkeley National Laboratory

Title

LINAC DESIGN FOR AN ARRAY OF SOFT X-RAY FREE ELECTRON LASERS

Permalink

<https://escholarship.org/uc/item/9pq0j1zp>

Author

Zholents, Alexander A.

Publication Date

2008-11-18

LINAC DESIGN FOR AN ARRAY OF SOFT X-RAY FREE ELECTRON LASERS*

A.A. Zholents[#], E. Kur, G. Penn, Ji Qiang, M. Venturini, R. P. Wells, LBNL, Berkeley, CA 94720, U.S.A.

Abstract

The design of the linac delivering electron bunches into ten independent soft x-ray free electron lasers (FELs) producing light at 1 nm and longer wavelengths is presented. The bunch repetition rate in the linac is 1 MHz and 100 kHz in each of ten FEL beam lines. Various issues regarding machine layout and lattice, bunch compression, collimation, and the beam switch yard are discussed. Particular attention is given to collective effects. A demanding goal is to preserve both a low beam slice emittance and low slice energy spread during acceleration, bunch compression and distribution of the electron bunches into the array of FEL beamlines. Detailed studies of the effect of the electron beam microbunching caused by longitudinal space-charge forces and coherent synchrotron radiation (CSR) have been carried out and their results are presented.

LATTICE AND DESIGN PARAMETERS

The accelerator is schematically shown in Figure 1. It consists of an injector, a laser heater, a bunch compressor, two main linacs, a harmonic linearizer linac, and a beam switch yard (spreader) into ten FELs (not shown).

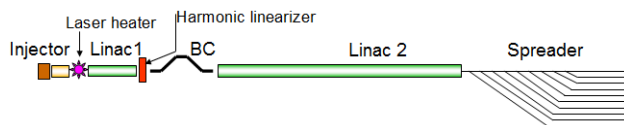


Figure 1. A schematic of the accelerator. Elements of the machine include the injector, laser heater, first linac, harmonic linearizer, bunch compressor, second linac, and spreader. The entire length of the machine is ~ 650 m.

The electron beam energy after injector at the entrance of the laser heater (LH) is ~ 40 MeV and the peak current is ~ 70A. The electron peak current after bunch compressor (BC), located behind the first linac (L1) and harmonic linearizer (HL) at a ~ 250 MeV beam energy point, is ~ 1 kA. The requirement for tunability of FELs outputs using APPLE-II undulator with adjustable helicity, in particular the FELs covering wavelengths from 1.5 nm to 1 nm, largely determines the lowest final beam energy ~ 2.4 GeV at the exit of the second linac (L2). However, somewhat surprisingly, we found that this energy only weakly depends on a size of a minimal gap in APPLE-II undulator [1] (see Figure 2).

According to the user requirements the accelerator must accommodate with sufficient flexibility three operation modes depending on the x-ray pulse length, i.e the long pulse from 500 fs to 100 fs, the medium pulse from 100 fs to 10 fs and the short pulse of 10 fs and shorter. Because

of a limited space, only the long bunch option is discussed here in detail. Other important electron beam parameters include the normalized slice electron beam emittance < 1 μm and the slice rms energy spread ~ 100 keV.

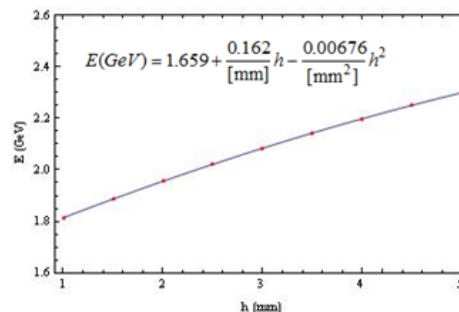


Figure 2. The electron beam energy that supports production of the x-rays within the range of wave lengths from 1 nm to 1.5 nm as a function of the size of the beam-stay-clear gap h in APPLE-II undulator.

Figure 3 shows one plausible alignment for a linac tunnel leading into the array of FELs located on the existing flat site in LBNL previously occupied by BEVATRON. It is also possible to begin the tunnel at a further point allowing more space for a linac.

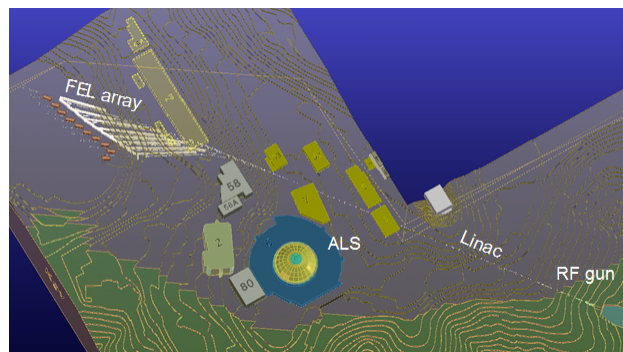


Figure 3. Bird view on East tunnel option for a linac, spreader and FEL array.

The linac lattice beginning functions beginning from the end of the injector are shown in Figure 4. Large beta-functions are used in several locations along the L2 for convenience of the collimation of halo particles. This is important as we plan for up to 1 mA average electron current. A small horizontal beta-function <10 m is used at the forth bending magnet of the bunch compressor in order to minimize the impact of CSR on the beam emittance. It is considered that TESLA cryomodules with 1.3 GHz linac structures will be used in L1 and L2 with the energy gain of 13.5 MeV/m in the active part. However, it is worth pointing out that cryomodules with

*Work supported by the U.S. Department of Energy under Contract No. DE-AC02-05CH11231.

[#]AZholents@lbl.gov

1.5 GHz linac structures under development for the CEBAF upgrade could also be used.

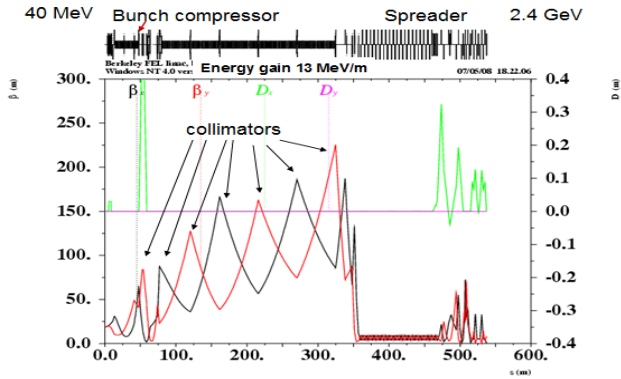


Figure 4. Linac lattice beginning from the end of the injector.

L1 is followed by HL which is a 3.9 GHz superconducting linac with the energy gain of 5 MeV/m and a total energy of ~ 30 MeV. HL is used to decelerate the electrons and (together with L1) to produce the linear energy chirp in the electron bunch in front of the BC. BC has a large $R56=0.135$ m and produces bunch compression increasing the electron peak current up to 1 kA. Fine tuning of the rf amplitudes and phases in L1 and HL is needed in order to obtain a desirable compression as seen in Figure 5. BC is followed by L2 and the switch

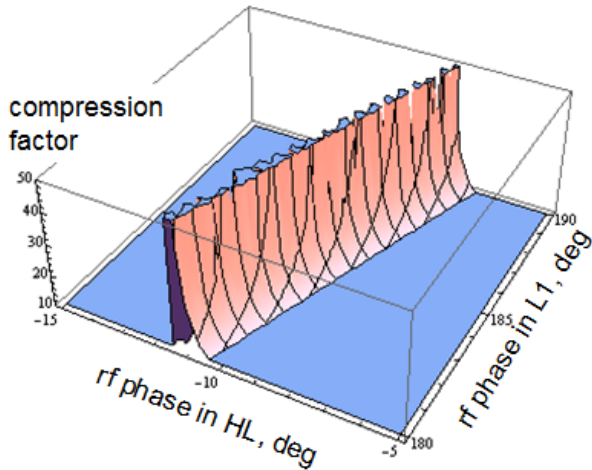


Figure 5. Compression factor (CF) as a function of the rf phases in linac L1 and HL. Steep rise of CF indicates high sensitivity to all parameters.

yard we call a “spreader”, which distributes electron bunches into ten independent FEL undulator lines. The maximum bunch repetition rate in the linac is 1 MHz and 100 kHz in each of ten FEL beam lines.

Figure 6 shows a schematic of the beam take-off section of the spreader. Each beamline has a 2 m long stripline kicker with a 5 mm gap providing maximum kick of 3 mrad at a 100 kHz pulse repetition rate and a 2 m long electromagnet septum located at a 90° betatron phase advance with respect to the kicker and providing 27 mrad turn to the beam. The septum is followed by three quads, bending magnet another three quads and another bend

magnet (see, Figure 7). All these plus the kicker and a septum make the triple bend achromatic and isochronous lattice. This is considered to be important in order to minimize the impact of the bending on the beam microbunching [2].

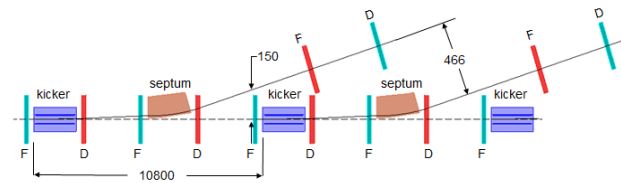


Figure 6. Beam take-off section of the spreader. Only two out of ten neighboring beamlines are shown.

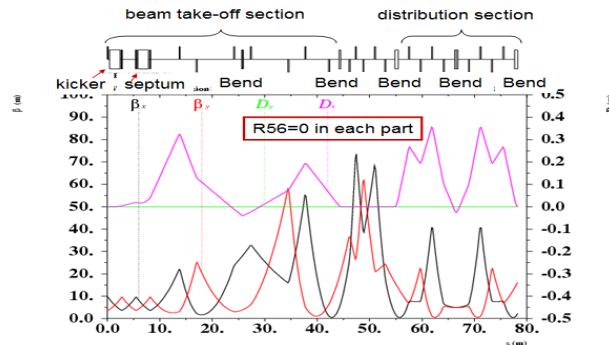


Figure 7. Lattice of the beam take-off section of the spreader. The downstream beam distribution section is also shown. This section is specific for each FEL and is used to fan out all FEL lines by turning the electron beam at various angles, but all of them have a similar design and are achromatic and isochronous.

COLLECTIVE EFFECTS

A major emphasis in the linac design was given to understanding, characterization and control of collective effects caused by the space charge, rf structure wake-fields, and CSR. The approach taken include analytical estimations, reverse tracking in longitudinal phase space [3], fine tuning by tracking of a small number of macroparticles in 3D phase space and performance validation with tracking up to one billion macroparticles. For these tasks we used a package of computer codes: LiTrack [4], Elegant [5], Vlasov solver [6], CSRTrack [7], and IMPACT [8].

First we verified a concept of the spreader lattice by tracking particles from the end of BC to the end of the linac and through the spreader using a flat top, 0.8 ps long electron bunch with 1 kA peak current. We found no evidence for slice emittance growth and for microbunching instability.

The result of the particle tracking through the entire machine beginning from the end of the injector is shown in Figures 10 and 11. The simulation was carried out for a 0.8 nC electron bunch with 70 A initial peak current and parabolic density distribution. It is assumed that LH will be used for control of the energy spread after injector and 5 keV rms energy spread was used in simulation. We note

that after accounting for a compression factor of ~ 20 , the modulation period due to microbunching instability seen

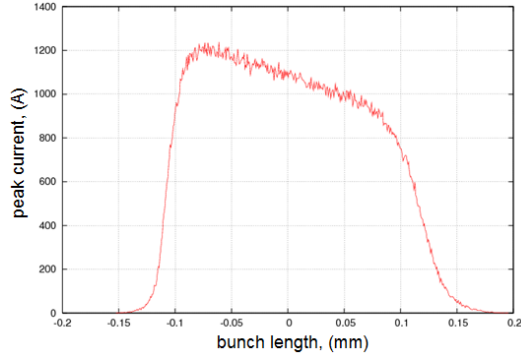


Figure 10. Peak current distribution at the end of the spreader obtained in tracking of 1B macroparticles through the entire machine beginning from the end of the injector using IMPACT.

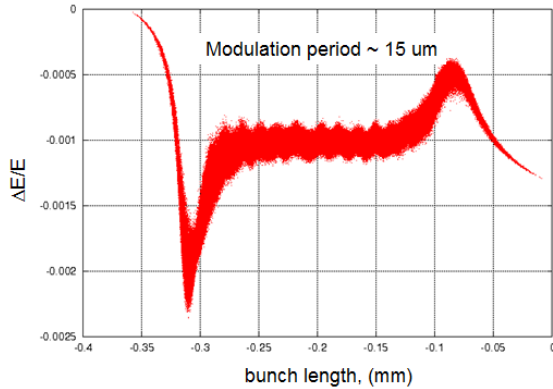


Figure 11. Longitudinal phase space at the end of the spreader obtained in tracking of 1B macroparticles through the entire machine beginning from the end of the injector using IMPACT.

in Figure 11 is in a good agreement with analysis of the gain of the microbunching instability performed on the basis of the linear theory [9] (see, Figure 12).

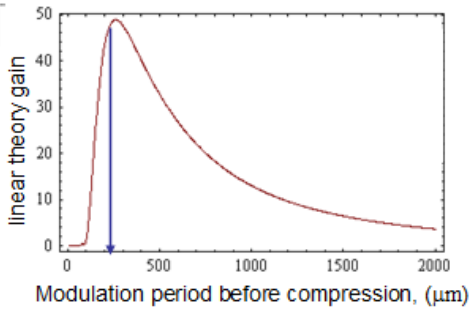


Figure 12. Gain of the microbunching instability. Arrow indicates modulation period obtained in macroparticle tracking (after accounting for a compression factor).

Figure 13 shows the normalized slice emittance at the end of the spreader which is the same as $0.45 \mu\text{m}$ initial emittance assumed in this simulation.

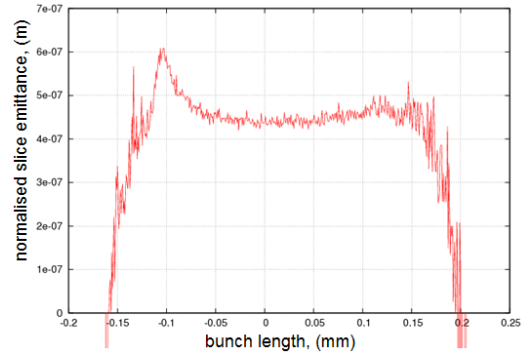


Figure 13. Normalized slice emittance at the end of the spreader obtained in tracking of 1B macroparticles through the entire machine beginning from the end of the injector using IMPACT.

Finally, Figure 14 shows the rms slice energy spread at the end of the spreader. For the most part of the bunch it is simply defined by the bunch compression and is not affected by microbunching instability. The large increase at the tail of the bunch is due to off-set of the central slice energy seen in Figure 10.

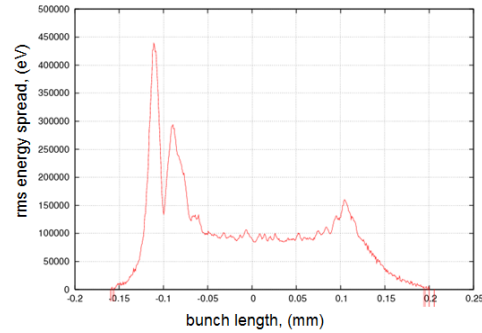


Figure 14. Slice rms energy spread at the end of the spreader obtained in tracking of 1B macroparticles through the entire machine beginning from the end of the injector using IMPACT.

In conclusion, we have produce a design for an accelerator satisfying performance requirements for soft x-ray FEL array. Testing this design by particle tracking indicates that all adverse collective effects are well managed. This allows the electron beam transport from injector to FELs without deterioration of the slice emittance and slice energy spread.

REFERENCES

- [1] A. Zholents, CBP Tech. Note – 381, (2007).
- [2] M. Venturini, A. Zholents, NIM A, **593**, 53(2008).
- [3] M. Cornacchia *et al.*, PRST-AB, **9**, 120701(2006).
- [4] K. L. F. Bane and P. Emma, Proc. Part. Acc. Conf., Knoxville, Tennessee, 4266(2005).
- [5] M. Borland, APS Tech. Note LS-207, (2000).
- [6] M. Venturini, *et al.*, PRST-AB, **10**, 05403 (2007).
- [7] M. Dohlus, TESLA-FEL-2003-05, DESY, 2003.
- [8] J. Qiang, *et al.*, J. Comp. Phys. **163**, 434 (2000).
- [9] S. Heifets, *et al.*, PRST-AB, **5**, 064401 (2002).